Aberrator prism profile recognition with convolutional neural networks for transcranial ultrasound investigation

A.V. Vasyukov, A.S. Stankevich, K.A. Beklemysheva, I.B. Petrov
Moscow Institute of Physics and Technology

November 03, 2021

Mathematical Models and Numerical Methods in Biology and Medicine, XIII conference, INM RAS

Motivation

Aberrations

Ultrasound investigation in heterogeneous medium can be hampered by aberrations

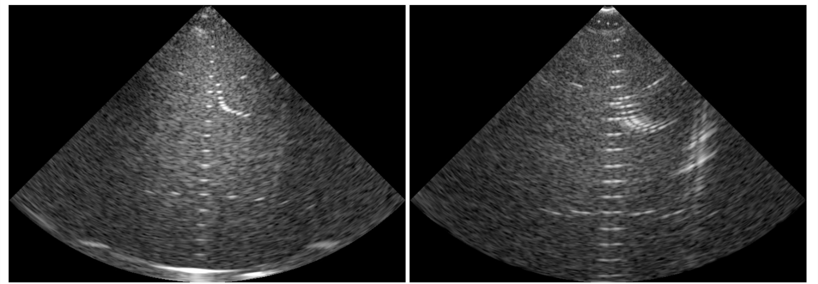

Figure 1: Medical phantom without aberrator (left) and through test aberrator (right)

(The experimental data was provided by the group of Kulberg N.S. from Moscow Research and Practical Centre of Medical Radiology)

Aberrations root cause

Ultrasound waves in heterogeneous medium are reflected and refracted multiple times by the boundaries.

Sample: ultrasound waves in a notched prism near the boundary of the medium.

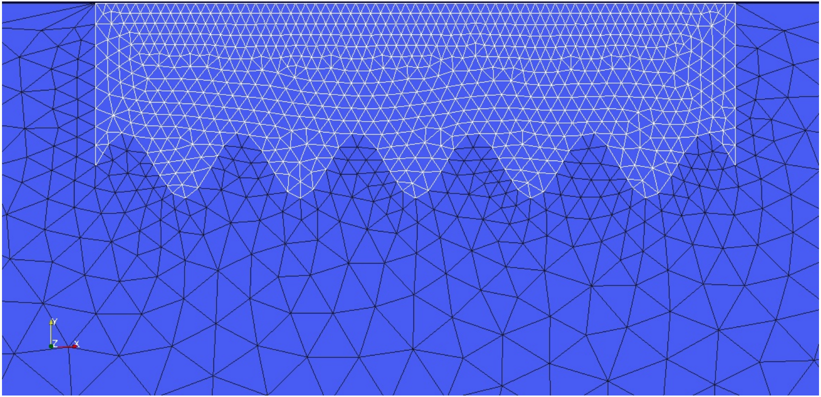

Aberrations root cause

Ultrasound waves in heterogeneous medium are reflected and refracted multiple times by the boundaries.

Sample: ultrasound waves in a notched prism near the boundary of the medium.

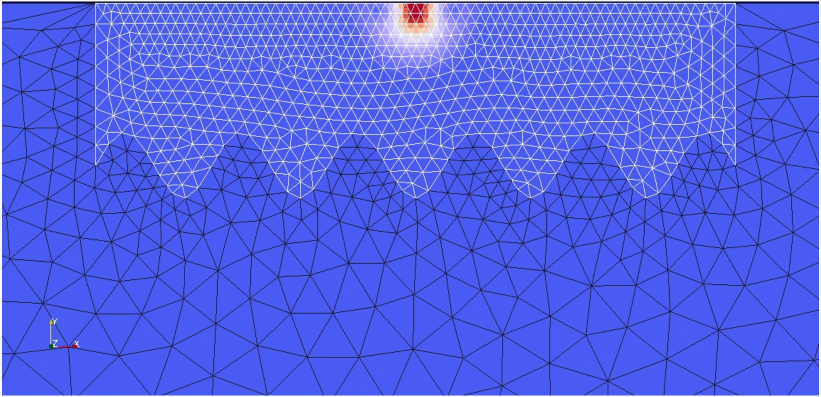

Aberrations root cause

Ultrasound waves in heterogeneous medium are reflected and refracted multiple times by the boundaries.

Sample: ultrasound waves in a notched prism near the boundary of the medium.

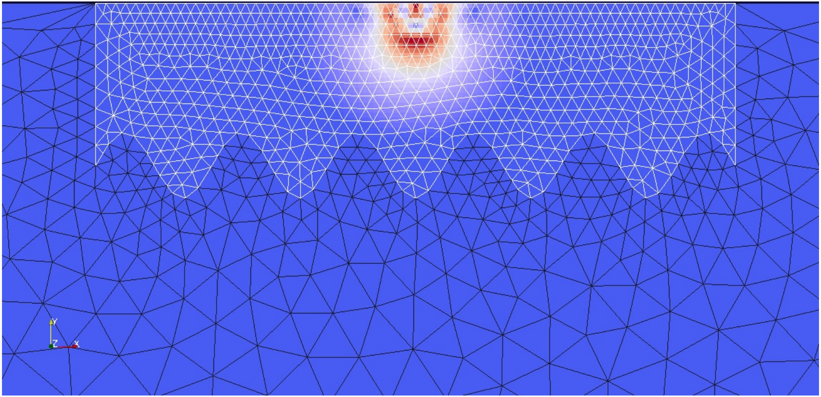

Aberrations root cause

Ultrasound waves in heterogeneous medium are reflected and refracted multiple times by the boundaries.

Sample: ultrasound waves in a notched prism near the boundary of the medium.

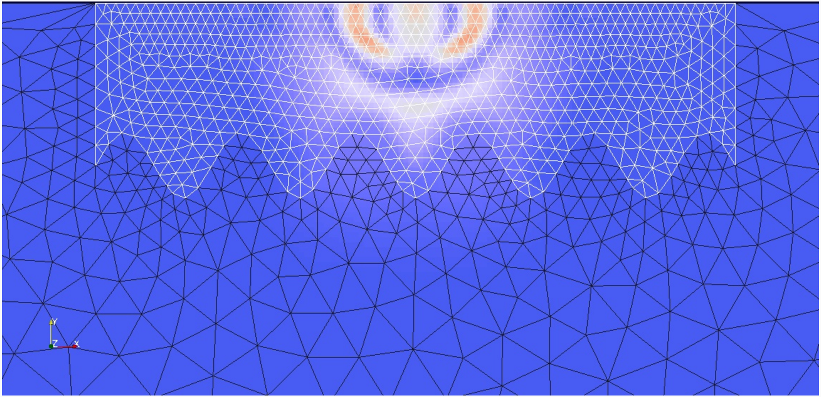

Aberrations root cause

Ultrasound waves in heterogeneous medium are reflected and refracted multiple times by the boundaries.

Sample: ultrasound waves in a notched prism near the boundary of the medium.

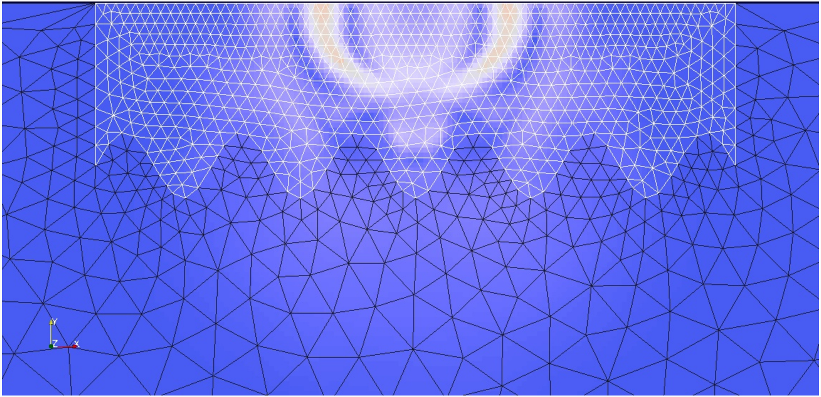

Aberrations root cause

Ultrasound waves in heterogeneous medium are reflected and refracted multiple times by the boundaries.

Sample: ultrasound waves in a notched prism near the boundary of the medium.

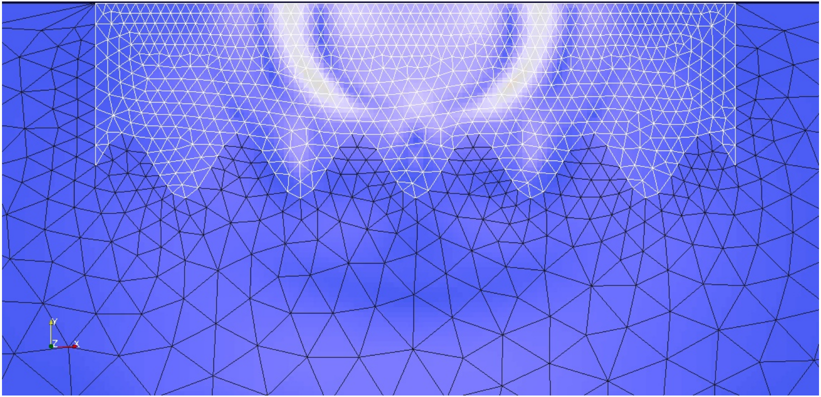

Aberrations root cause

Ultrasound waves in heterogeneous medium are reflected and refracted multiple times by the boundaries.

Sample: ultrasound waves in a notched prism near the boundary of the medium.

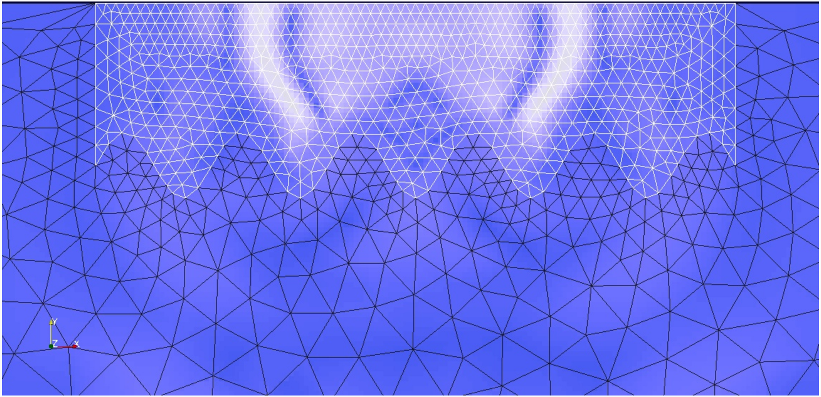

Aberrations root cause

Ultrasound waves in heterogeneous medium are reflected and refracted multiple times by the boundaries.

Sample: ultrasound waves in a notched prism near the boundary of the medium.

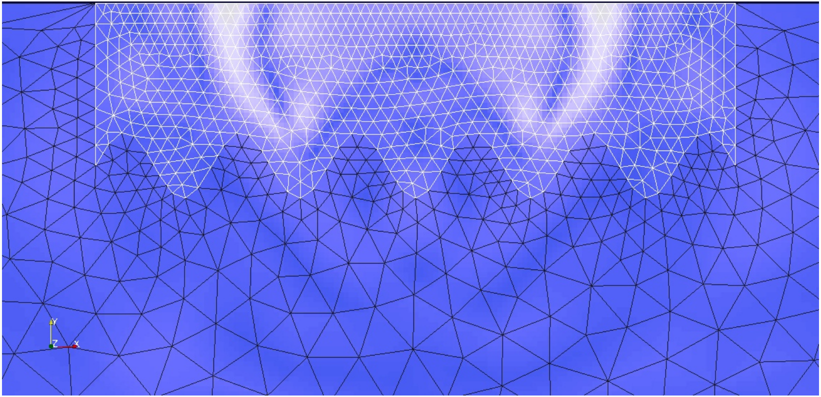

Aberrations root cause

Ultrasound waves in heterogeneous medium are reflected and refracted multiple times by the boundaries.

Sample: ultrasound waves in a notched prism near the boundary of the medium.

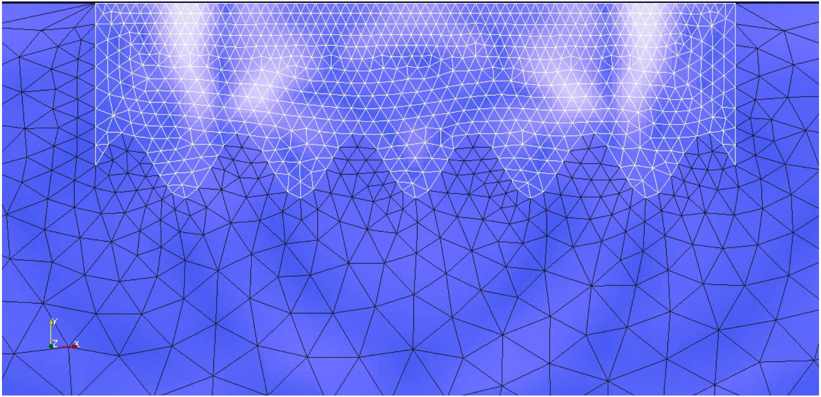

Aberrations root cause

Ultrasound waves in heterogeneous medium are reflected and refracted multiple times by the boundaries.

Sample: ultrasound waves in a notched prism near the boundary of the medium.

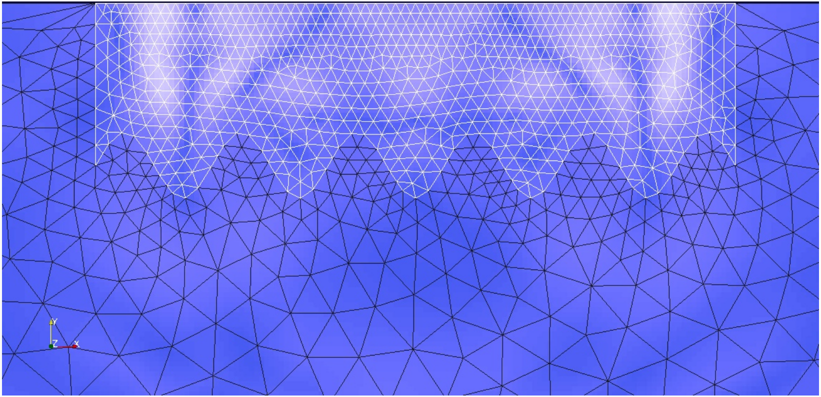

Aberrations root cause

Sample: ultrasound waves fronts in heterogeneous medium.

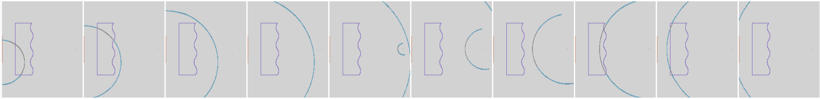

Figure 2: Ultrasound waves fronts. The prism has higher sound speed than the surrounding medium (top row), the same sound speed (medium row), lower sound speed (bottom row).

Aberrations root cause

Sample: ultrasound waves fronts in heterogeneous medium.

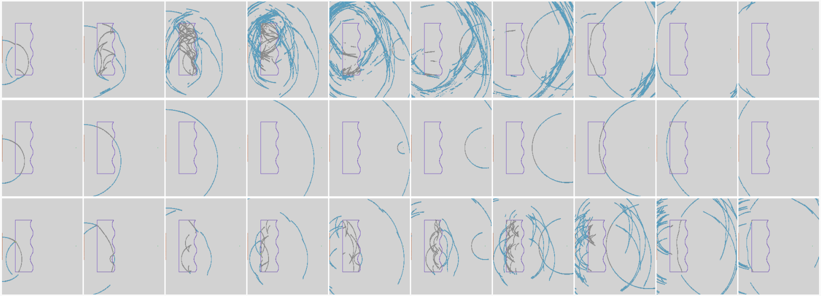

Figure 2: Ultrasound waves fronts. The prism has higher sound speed than the surrounding medium (top row), the same sound speed (medium row), lower sound speed (bottom row).

Direct problem

Mathematical model

Full dynamic system of equations of viscoelasticity for anisotropic medium.

$$\frac{\partial v_x}{\partial t} = \frac{1}{\rho}(\frac{\partial \sigma_{xx}}{\partial x} + \frac{\partial \sigma_{xy}}{\partial y} + \frac{\partial \sigma_{xz}}{\partial z})$$
$$\frac{\partial v_y}{\partial t} = \frac{1}{\rho}(\frac{\partial \sigma_{xy}}{\partial x} + \frac{\partial \sigma_{yy}}{\partial y} + \frac{\partial \sigma_{yz}}{\partial z})$$
$$\frac{\partial v_z}{\partial t} = \frac{1}{\rho}(\frac{\partial \sigma_{xz}}{\partial x} + \frac{\partial \sigma_{yz}}{\partial y} + \frac{\partial \sigma_{zz}}{\partial z})$$
$$\frac{\partial \sigma_{xx}}{\partial t} = c_{11}\frac{\partial v_x}{\partial x} + c_{12}\frac{\partial v_y}{\partial y} + c_{13}\frac{\partial v_z}{\partial z} + c_{14}(\frac{\partial v_z}{\partial y} + \frac{\partial v_y}{\partial z}) + c_{15}(\frac{\partial v_z}{\partial x} + \frac{\partial v_x}{\partial z}) + c_{16}(\frac{\partial v_y}{\partial x} + \frac{\partial v_x}{\partial y}) - \frac{\sigma_{xx}}{\tau_0}$$
$$\frac{\partial \sigma_{yy}}{\partial t} = c_{12}\frac{\partial v_x}{\partial x} + c_{22}\frac{\partial v_y}{\partial y} + c_{23}\frac{\partial v_z}{\partial z} + c_{24}(\frac{\partial v_z}{\partial y} + \frac{\partial v_y}{\partial z}) + c_{25}(\frac{\partial v_z}{\partial x} + \frac{\partial v_x}{\partial z}) + c_{26}(\frac{\partial v_y}{\partial x} + \frac{\partial v_x}{\partial y}) - \frac{\sigma_{yy}}{\tau_0}$$
$$\frac{\partial \sigma_{zz}}{\partial t} = c_{13}\frac{\partial v_x}{\partial x} + c_{23}\frac{\partial v_y}{\partial y} + c_{33}\frac{\partial v_z}{\partial z} + c_{34}(\frac{\partial v_z}{\partial y} + \frac{\partial v_y}{\partial z}) + c_{35}(\frac{\partial v_z}{\partial x} + \frac{\partial v_x}{\partial z}) + c_{36}(\frac{\partial v_y}{\partial x} + \frac{\partial v_x}{\partial y}) - \frac{\sigma_{zz}}{\tau_0}$$
$$\frac{\partial \sigma_{yz}}{\partial t} = c_{14}\frac{\partial v_x}{\partial x} + c_{24}\frac{\partial v_y}{\partial y} + c_{34}\frac{\partial v_z}{\partial z} + c_{44}(\frac{\partial v_z}{\partial y} + \frac{\partial v_y}{\partial z}) + c_{45}(\frac{\partial v_z}{\partial x} + \frac{\partial v_x}{\partial z}) + c_{46}(\frac{\partial v_y}{\partial x} + \frac{\partial v_x}{\partial y}) - \frac{\sigma_{yz}}{\tau_0}$$
$$\frac{\partial \sigma_{xz}}{\partial t} = c_{15}\frac{\partial v_x}{\partial x} + c_{25}\frac{\partial v_y}{\partial y} + c_{35}\frac{\partial v_z}{\partial z} + c_{45}(\frac{\partial v_z}{\partial y} + \frac{\partial v_y}{\partial z}) + c_{55}(\frac{\partial v_z}{\partial x} + \frac{\partial v_x}{\partial z}) + c_{56}(\frac{\partial v_y}{\partial x} + \frac{\partial v_x}{\partial y}) - \frac{\sigma_{xz}}{\tau_0}$$
$$\frac{\partial \sigma_{xy}}{\partial t} = c_{16}\frac{\partial v_x}{\partial x} + c_{26}\frac{\partial v_y}{\partial y} + c_{36}\frac{\partial v_z}{\partial z} + c_{46}(\frac{\partial v_z}{\partial y} + \frac{\partial v_y}{\partial z}) + c_{56}(\frac{\partial v_z}{\partial x} + \frac{\partial v_x}{\partial z}) + c_{66}(\frac{\partial v_y}{\partial x} + \frac{\partial v_x}{\partial y}) - \frac{\sigma_{xy}}{\tau_0}$$

Numerical methods

- grid-characteristic method (viscoelasticity);
- discontinuous Galerkin method (elasticity);
- ray tracing / wavefront reconstruction (acoustics).

Phased array

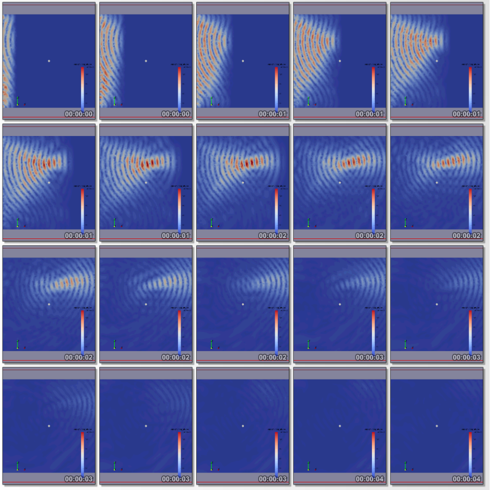

Figure 3: Phased array pulse focusing in viscoelastic medium

3D geometry

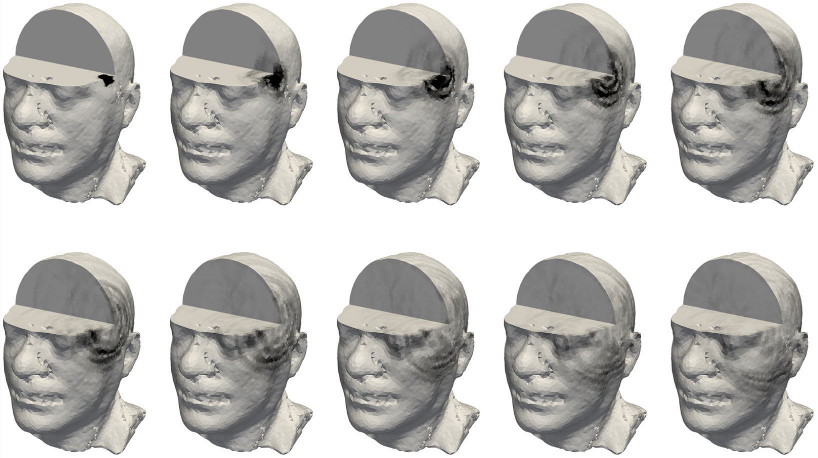

Figure 4: Ultrasound pulse in segmented 3D head model

(The geometry, segmentation and mesh were provided by the group of Vassilevski Y.V. from INM RAS.)

Validation

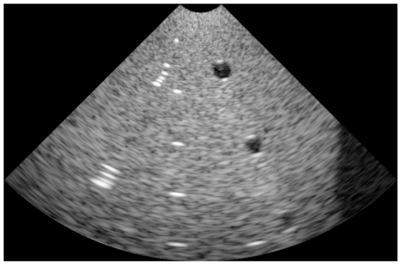

Figure 5: Experimental results

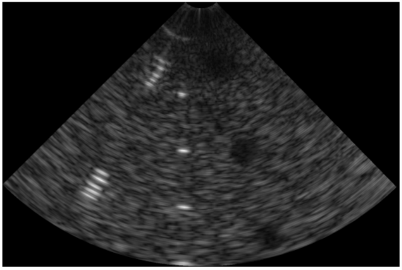

Figure 6: Numerical results

Modeling aberrations

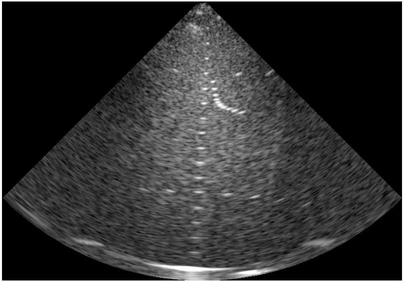

Figure 7: Medical phantom (experimental data)

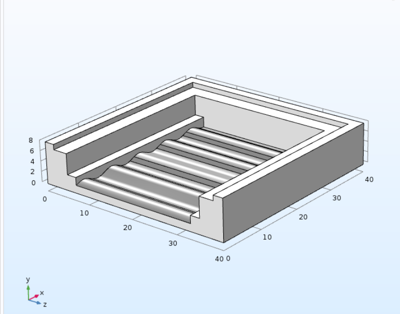

Figure 8: Notched aberrator model

Modeling aberrations

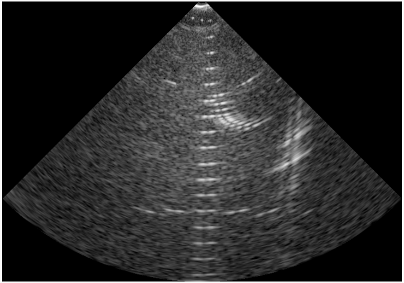

Figure 9: Experimental results

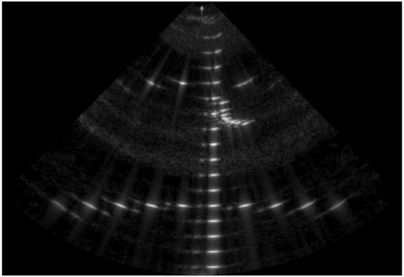

Figure 10: Numerical results

(Numerical results consider aberrator and bright pins only, grey background is omitted for faster calculations.)

Inverse problem

Current target problem

Aberrator position identification:

- 2D case;
- two subdomains with constant Lame coefficients and density;
- linear phased array, single element emits, all elements receive.

Numerical approach

- SegNet-like architecture.
- Network predicts probability of the node to belong to first subdomain.
- Weighted binary cross entropy loss function.
- Optimization via backprop with AdamW algorithm with constant learning rate.

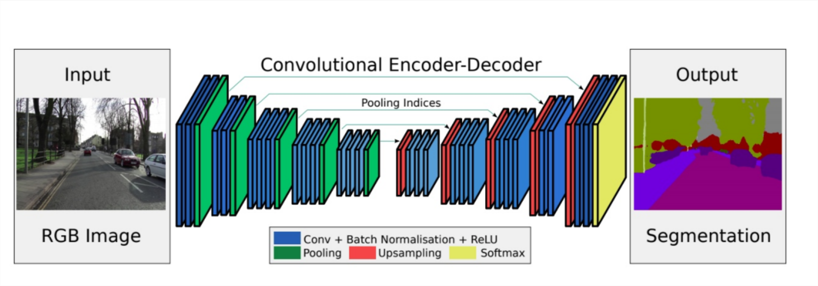

Figure 11: Classical SegNet pipeline

Numerical approach

- SegNet-like architecture.
- Network predicts probability of the node to belong to first subdomain.
- Weighted binary cross entropy loss function.
- Optimization via backprop with AdamW algorithm with constant learning rate.

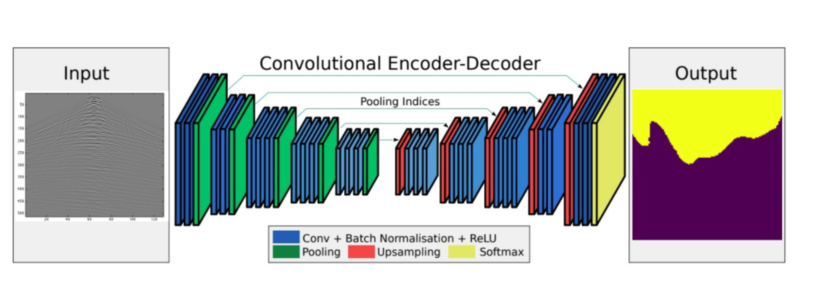

Figure 12: Our pipeline

Case 1: sin-waved aberrator

Numerical approach

- 2000 direct problems simulations with discontinuous Galerkin method
- Convolutional neural network (SegNet-like) is trained using the simulated data
- Train set: square domain, sin-formed aberrator with different parameters
- Test set: similar samples with different parameters

Results

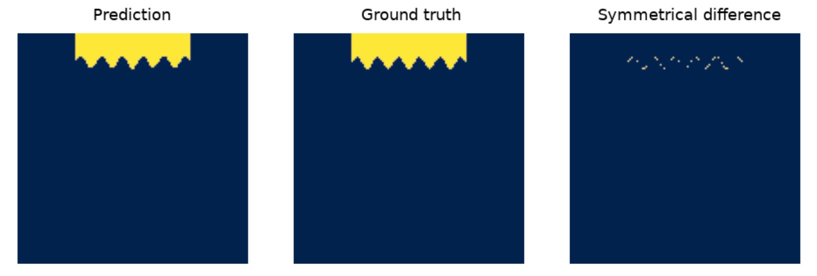

Jaccard index: 0.94

Case 2: complex aberrator

Numerical approach

- 2000 direct problems simulations with discontinuous Galerkin method
- Convolutional neural network (SegNet-like) is trained using the simulated data
- Train set: square domain, random non-smooth curves splitting the domain into parts
- Test set: sinusoidal and straight borders (never seen in train set)

Validation

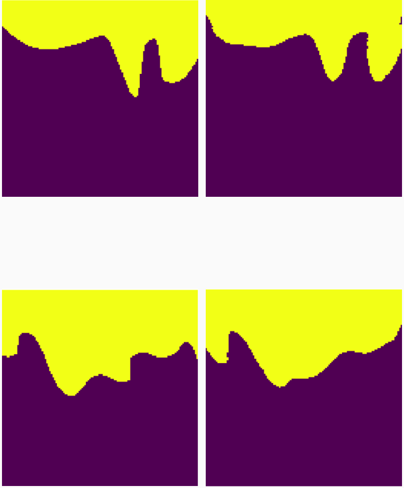

Testing

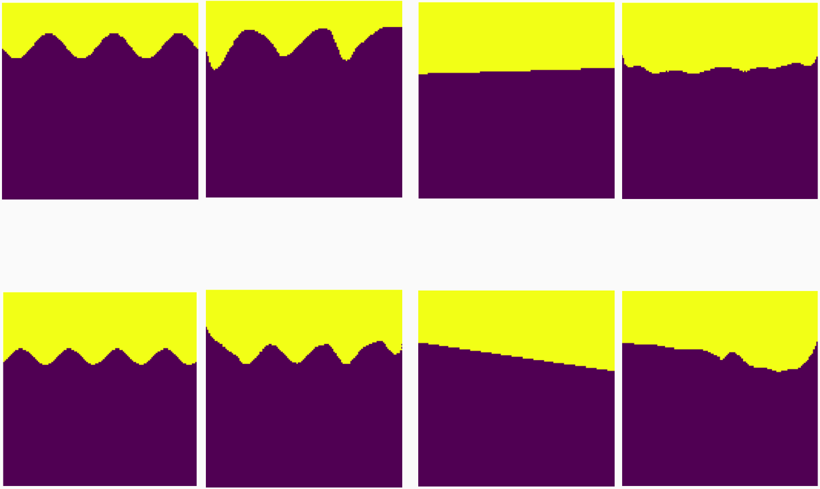

Case 3: learning velocity model

Numerical approach

- 1600 direct problems simulations with grid-characteristic method
- 9 shots per sample
- Convolutional neural network (UNet-like) is trained using the simulated data
- Learning velocity model, not just binary classification problem

Sample velocity models

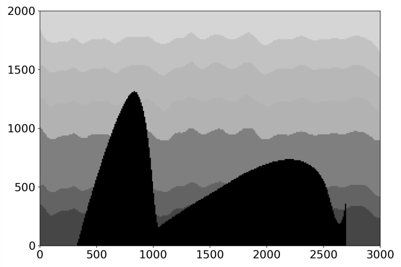

Figure 13: Typical model 1

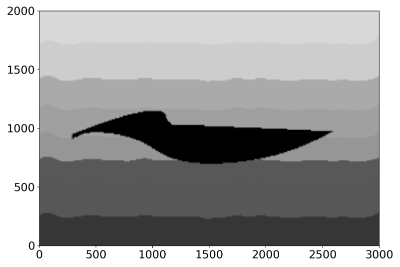

Figure 14: Typical model 2

Prediction results

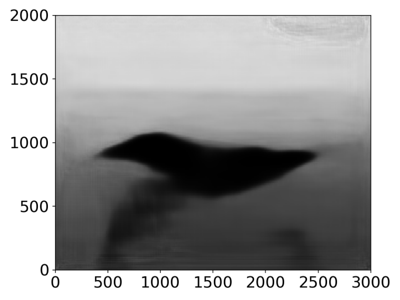

Figure 15: Baseline model

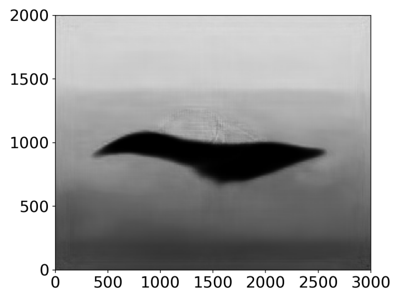

Figure 16: Model with Fourier images

SSIM: 0.93

Results

Current results:

- CNNs can work in real time;
- reasonable initial results for the boundary location and velocity model problems.

Future work:

- combine numerical and experimental data;
- use CNN output as an initial guess for gradient optimization;
- restore the aberrated data having the boundary location data.

Thank you!